# Complementary Ion Beam Analysis and Raman Studies for Investigation of the Carbon Coating Impact on Li Insertion/Deinsertion Process at LiFePO_4/C Electrodes

Suzy Surblé, Aurelien Habrioux, Cyril Paireau, Pascal Berger, Hicham Khodja, Delphine Neff, Dominique Gosset, Sophie Mailley, Sébastien Patoux

# Complementary Ion Beam Analysis and Raman Studies for Investigation of the Carbon Coating Impact on Li Insertion/Deinsertion Process at $LiFePO_4$/C Electrodes

**Suzy Surblé, Aurélien Habrioux, Cyril Paireau, Pascal Berger, Hicham Khodja, Delphine Neff, Dominique Gosset, Sophie Mailley, and Sébastien Patoux**

*LEEL, NIMBE, CEA, CNRS, Université Paris-Saclay, CEA Saclay 91191 Gif-sur-Yvette, France*
*LAPA, NIMBE-IRAMAT, CEA, CNRS, Université Paris-Saclay, CEA Saclay 91191 Gif-sur-Yvette, France*
*CEA/DEN/DANS/DMN/SRMA/LA2M, F-91191 Gif-sur-Yvette, France*
*CEA / LITEN / DEHT / L2MB, 38054 Grenoble cedex 9, France*

Electrode materials were prepared using two commercial C-$LiFePO_4$ powders (called hereafter LFP-A and LFP-B). The nature and the thickness of carbon coating have been characterized by Raman spectroscopy and Transmission Electron Microscopy. The carbon coating of the LFP-B is more graphitized than LFP-A, which appears amorphous. The lithium distribution of these electrodes is investigated using ion beam techniques as a function of its state of charge (SOC). The nuclear microanalyses reveal the presence of different dopings in the active materials (Ti or V). A layer richer in carbon (in addition to the composite electrode) is systematically observed on LFP-A pristine and cycled electrodes. In both materials, immobilization of lithium is visible. Higher content of lithium was observed for the LFP-B electrode.

Numerous studies have paid attention to $LiFePO_4$ active material since its discovery in 1997 by Padhi et al.[1] This material is a promising candidate for large scale applications in reason of its non-toxicity, low cost and cycling stability.[2–4] However, its low electronic conductivity ($10^{-9}$ S $cm^{-1}$)[5–7] leads to poor electrochemical performances at high cycling rates. To circumvent this difficult , several possibilities have been explored. Among them particle size reduction is of upmost importance since it allows reducing transport distance for both Li ions and electrons.[8–11] Other ways to improve intrinsic electronic conductivity of the material are supervalent cations doping, which allows elevating both $Li^+$ diffusion coefficien in the host matrix and its electronic conductivity,[12] or carbon coating.[13,14] The latter enhances the surface electronic conductivity of the active particles. High cycling rate capability of $LiFePO_4$ is thus improved since the presence of such a coating promotes both fast $Li^+$ diffusion to or from the $LiFePO_4$ phase and electrons tunneling from the carbon to the $FePO_4$ / $LiFePO_4$ front phase in the material.[15] Carbon coating is also used both to reduce particle sintering during the synthesis and to protect the active material from surface side reactions with the electrolyte.[16]

Nevertheless, it has been observed that species composing the passivation layer would grow onto the surface of carbon coating, which seems to indicate that carbon could play a significan role for catalytic electrolyte decomposition. Even if the phenomenon is more limited in the case of the carbon-coated material, the growth of this interface could be at the origin of cluster insulating leading to capacity fading. Here, we present the study of two commercial carbon coated $LiFePO_4$. Original characterizations are presented using ion beam techniques. Nuclear microprobe has been depicted in previous works as a powerful tool capable of simultaneously and directly tracking all the elements composing a C-$LiFePO_4$ based electrodes as a function of its state of charge (SOC).[17,18] It especially allows visualizing the whole amount of Li contained in the electrode as well as localizing these atoms in the electrode film Consequently, a direct observation of Li-based products forming the SEI is possible. In order to link the observed products with structural properties, thickness and porosity of the different carbon coatings, these latter were investigated by Raman spectroscopy and High-Resolution Transmission Electron Microscopy (HRTEM).

## Experimental

***Materials preparation.***—C-$LiFePO_4$ commercial powders with different carbon coatings were purchased from different companies and were used as received (called respectively LFP-A and LFP-B). In all cases, the positive electrode was prepared by realizing slurry composed of 90.5 wt% of C-$LiFePO_4$ active powder, 2.5 wt% of VGCF fibers 2.5 wt% of carbon black and 4.5 wt% of polyvinylidene fluorid (PVDF), which acts as a binder. Lithium ion cells were then assembled by using a $LiFePO_4$ electrode as cathode and a $Li_4Ti_5O_{12}$ based electrode as anode. Celgard 2400 and 1 M $LiPF_6$ dissolved in 1:1 ethylene carbonate/dimethylcarbonate were respectively used as separator and electrolyte. After 3 cycles (charge and discharge) at C/20 rate and 6 cycles at C/10 rate, the different electrodes were charged to different states of charge (SOC 0%, 25%, 50%, 75% and 100%) at a C/10 rate. The electrodes were then removed from the cell and rinsed with dimethylcarbonate to eliminate the residual electrolyte.

***Usual materials characterizations.***—X-ray diffraction patterns were collected using a Bruker D8 ADVANCE diffractometer. The experimental setup is equipped with a parabolic Göbel mirror on a line focus Cu radiation tube. XRD data were collected in the range 10–120° with a step of 0.028° and a count time of 1 second per step. XRD spectra were refine by Rietveld method using Fullprof software.[19] The background level was fitte with a fi e-order polynomial function and the peak shape with a pseudo-Voigt function.

The nanoparticles and the coating carbon were characterized by transmission electron microscopy (TEM) performed on a JEOL 2000FX or on a High Resolution Scanning Transmission Electron Microscope (HRSTEM) Titan.

To characterize chemical nature of the different carbon coatings, Raman spectroscopy analyses were carried out on an Invia Refl x spectrometer equipped with a laser emitting at 532 nm. The objective ×50 was used and the laser power on the sample was about 10 mW. The use of a 2400 g/mm grating delivered a spectral resolution of 2 $cm^{-1}$. Acquisitions on the sample lasted a few tenths of second.

***Ion beam analysis.***—The Saclay nuclear microprobe was used to characterize the chemical compositions of the active materials and the resulting electrodes as a function of its state of charge. First, the full chemical composition of a sample was obtained using different techniques (RBS, PIXE and PIGE) with a proton microbeam at 2600 keV. In order to confir the concentration of carbon, a 1350 keV deuteron microbeam was used. To stop deuteron backscattered particles, a 25 μm thick Mylar foil was set in front of the annular detector. Finally, all measurements were obtained by scanning the microbeam (spot size 2 × 2 $\mu m^2$) allowing 2D-distribution maps presenting lateral concentration variations for each element (map size 100 × 100 $\mu m^2$).

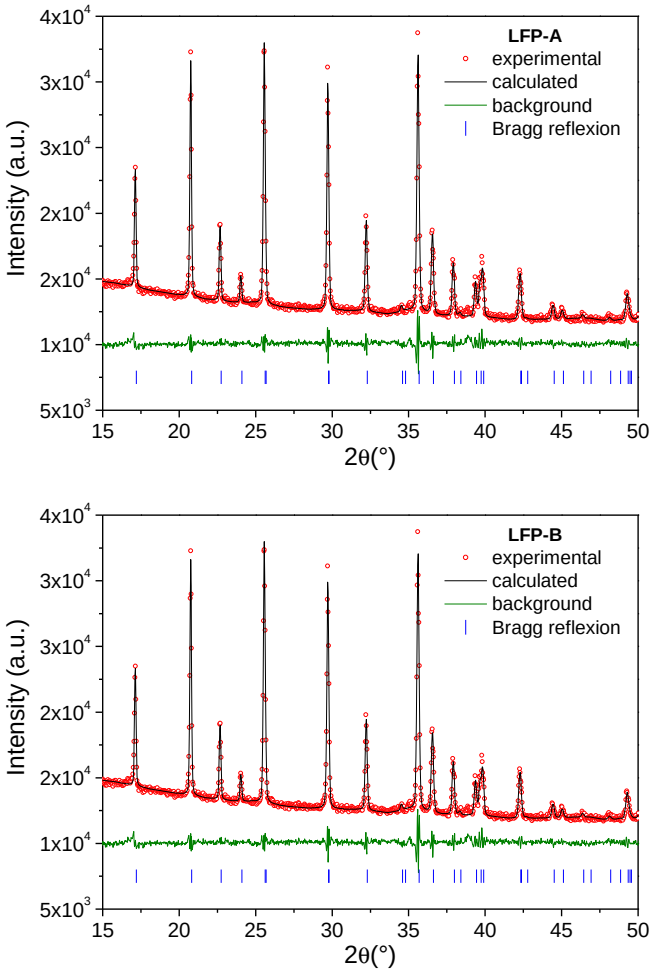


**Figure 1.** Rietveld refinemen of C-LiFePO$_4$ commercial powders.

## Results and Discussion

***Structure and morphology.***—X-ray diffraction patterns of LFP-A and LFP-B are shown in Fig. 1. All reflection in the XRD pattern were indexed to an orthorhombic structure (space group *Pnma*). A good agreement is observed between the experimental data and the simulated Rietveld patterns. The calculated lattice parameters are listed in Table I. The refine parameters are in agreement with the existing literature report in carbon-coated LiFePO$_4$ particles.[20] According to Chen et al.,[21] the cell volume may be used as a measure of the iron disorder. Here, the cell volumes are less than 291.5 Å$^3$, which indicates that the iron is completely ordered.

To improve electronic conductivity, a carbon coating associated with a metal doping is added to the LiFePO$_4$ powders. In order to understand the carbon coating structure on the surface of the active material, we conduct TEM analysis of each commercial material. The nanoparticles of LFP-A powder contain some diffuse agglomerates with small sizes particles, while only nanoparticles are observed for LFP-B one (Figs. 2a–2d). The average particle sizes are in the range 100–2000 nm for LFP-A and 50–30 nm for LFP-B powder.

**Table I. Comparison of structural parameters obtained by Rietveld refinemen for active powder materials.**

| | a (Å) | b (Å) | c (Å) | V (Å$^3$) | $R_{wp}$ | $R_{bragg}$ |
|---|---|---|---|---|---|---|
| LFP-A | 10.305(5) | 5.993(2) | 4.682(6) | 289.15(1) | 1.74 | 4.68 |
| LFP-B | 10.304(2) | 5.995(3) | 4.686(1) | 289.46(5) | 1.47 | 4.18 |

In the two samples, the carbon layers both coat on the surface of the LiFePO$_4$. The carbon coating of LFP-A appears homogeneous with some clumps (Fig. 2b). The thickness of the layer is estimated to be in the range 2–100 nm. For the LFP-B powder, the thickness of the carbon coating is thinner (0.5–1.5 nm). The specifi surface area of both materials is determined by the BET (Brunauer Emmett Teller) method. It is 10.44 and 11.66 m$^2$ g$^{-1}$ for LFP-A and LFP-B respectively. Bigger specifi surface areas can increase the interface between the electrode material and the electrolyte, which also favors $Li^+$ diffusion.

***Electrochemical properties.***—The capacity and the cyclability of the LiFePO$_4$ electrodes were determined between 1.0 and 2.5 V by galvanostatic charge/discharge performed at C/10 rate. Fig. 3a compares the firs charge/discharge profile of the electrodes prepared with two C-LiFePO$_4$ commercial powders. The voltage difference between the charge and the discharge f at ( $\Delta V$) corresponds to the polarization of the cell. The values of $\Delta V$ are very small (56.3 mV and 39.1 mV for LFP-A and LFP-B respectively). LFP-B electrode has a smaller polarization than LFP-A one, but the difference is not significant The Fig. 3b shows the differential capacity *dQ/dE* as a function of the potential E for the initial and last cycles. The curves of LFP-A electrode appears less smooth than LFP-B ones but present some similarities (potential of the charge and discharge). The different peaks observed for the LFP-A can correspond to different electrochemical reactions which occur during the working of the battery. Note that LFP-A material displays a slightly higher discharge capacity of 155 mAh.g$^{-1}$ versus149 mAh.g$^{-1}$ for the LFP-B electrode. The irreversible capacities remain of the same order of magnitude (∼10 mAh/g) for the two insertion materials.

***Nature of the carbon coating.***—In order to probe structural information about lattice defects and long-range order of the graphitic lattice, Raman spectroscopy was employed.[22,23] The probing depth for carbon with this technique is approximately 30 nm.[24] Fig. 4 displays the Raman spectra of both C-LiFePO$_4$ powders in the range 800–2000 cm$^{-1}$. To determine characteristics of the bands associated with the carbon and to analyze its nature, decompositions of experimental spectra were performed using a combination of four Gaussian-Lorentzian bands.[25] After the determination of the baseline, the full width at half maximum (FWHM), the positions and the intensities of the bands were refined Results obtained are reported in Table II. The relatively small band at 956 cm$^{-1}$ corresponds to the $PO_4$ symmetric stretching vibration in triphylite structure.[26,27] No shift mode in terms of vibration frequency can be observed, but the intensity of this peak appears much higher in LFP-A powder compared to LFP-B one. According to the previous work of Julien et al.,[28] its intensity is related to the carbon amount present onto the surface of LiFePO$_4$. As no information on the carbon content was given by the providers of the powders, the total amount of carbon of each commercial powder is estimated using ion beam techniques (see section Nuclear microprobe analysis). LFP-A powder contains less carbon than LFP-B one (∼4.5 at.% for LFP-A and ∼8.1 at.% for LFP-B). The lines associated with the stretching vibration of $PO_4$ are therefore more intense.

The spectral region (1200–1600 cm$^{-1}$) clearly exhibits several overlapping lines, which are fingerprint of highly disordered carbon.[29] The firs one located around 1200 cm$^{-1}$ is commonly associated to polyene-like structure (with the presence of sp$^3$ rich phases).[30–32] The second one (near 1350 cm$^{-1}$) mainly corresponds to the D line ($A_{1g}$ mode) associated with disorder-allowed zone-edge modes of graphite.[33] This mode is indeed forbidden in perfect graphite and only becomes active in presence of disorder.[30] The third line centered at around 1520 cm$^{-1}$ is attributed to the presence of amorphous sp$^2$ phase.[34] Finally, the last band close to 1600 cm$^{-1}$ corresponds to the G line and is associated with the optically allowed $E_{2g}$ zone center mode of crystalline graphite. The position of this Raman line is higher than in ordered graphitic phases, and in this case it overlaps perfectly with the D' line. Generally, the more graphitized the carbon is, the more intense the G band is, compared to the D band. No significan

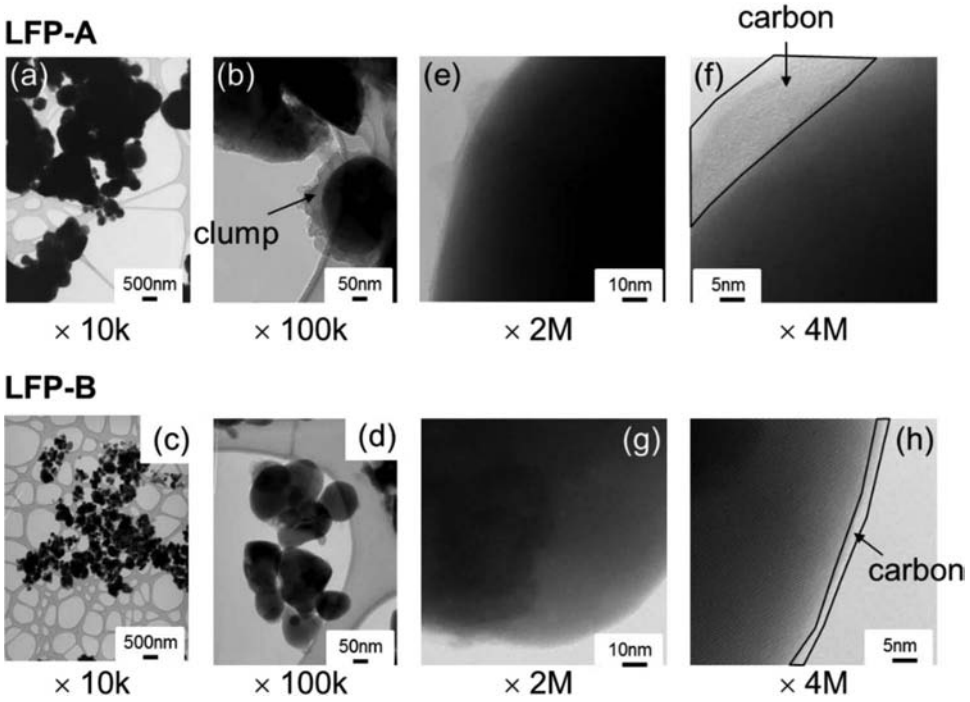


**Figure 2.** (a-d) Bright Field and (e-h) High Angle Annular Dark Field TEM images at different magnification for the two C-$LiFePO_4$ commercial powders.

shift in terms of band position could be observed ($\Delta\upsilon = 2$–$12$ $cm^{-1}$) between the two materials. The magnitude of the line centered at ca. 1520 $cm^{-1}$ is higher for the LFP-A electrode: its carbon coating is more disordered than the LFP-B one. As the FWHM values of the D bands are superior to 50 $cm^{-1}$, both electrodes have a poorly ordered carbon.[35] Tuinstra and Koenig[36] have proposed a relationship to determine the amount of defects in materials by determining the in-plane graphitic crystallite size. In particular, the intensity ratio of G to D band is inversely proportional to the in-plane crystallite size, $L_a$ (Eq. 1):

$$\frac{I_D}{I_G} = \frac{C(\lambda_{laser})}{L_a} \quad [1]$$

where $C(\lambda_{laser})$ is a variable scaling coefficien depending on $\lambda_{laser}$ and given by $C(\lambda_{laser}) = C_0 + \lambda_{laser}C_1$ (with $C_0 = -12.6$ nm and $C_1 = 0.033$, $\lambda_{laser} = 532$ nm).[37] The rather small values of $L_a$ (1.9 nm and 2.4 nm respectively for LFP-A and LFP-B) confir that the carbon is highly disordered.[38]

In principle, Raman spectra can provide information on $sp^2$ and $sp.^3$ As the $sp^2$ Raman cross section is 50–230 higher than the $sp^3$ one with visible exciting wavelength, multi-wavelength analysis is required to give reliable quantitative information on $sp^2/sp^3$ coordinated carbon ratio. In our work, the $sp^2/sp^3$ fraction is coarsely estimated using only one excitation line at 532 nm for Raman experiment. Thus, the following may be restricted to semi-quantitative discussion. The bands at ~1350 $cm^{-1}$ (D-band) and 1600 $cm^{-1}$ (G-band) were assigned to $sp^2$ graphite like structure and other two bands at ~1190 $cm^{-1}$ and 1525 $cm^{-1}$ to $sp^3$-like disordered carbon. Higher ratios $sp^2/sp^3$ were correlated to a more graphitic nature and higher electronic conductivity. The carbon coating of LFP-B electrode is more graphitized than the one of LFP-A which seems to be highly amorphous. According to Seid et al.,[39] the electronic transport in C-$LiFePO_4$ nanocomposite materials is limited by the $sp^3$ domains in the carbon coating and to inter-cluster contacts. This means that carbon coating formed onto the surface of LFP-B has a better electronic conductivity. This last observation is clearly in compliance with the evolution of the ratio of carbon to $PO_4$ band centered at 950 $cm^{-1}$. Actually, if we consider that Raman spectroscopy is a surface sensitive technique it is of evidence that results obtained allow to indicate the quality of the carbon coating. According to the study reported by Nakamura et al.,[27] a larger ratio of carbon to $PO_4$ bands clearly denotes a more uniform carbon coating. Moreover, the higher $I_D/I_G$ bands ratio suggests the presence of numerous defects and edges in the carbon coating of LFP-B, which may act as efficien catalytic sites where formation of decomposition compounds is greatly enhanced.

***Nuclear microprobe analyses.***—The spectrometry of the different interaction products of the ions of the beam with the target (charged particles, X-rays and γ-rays) allows the determination of elemental concentrations. The approach used to quantify lithium and carbon in our materials needs multiple data reduction from several ion beam conditions (2600 keV proton beam and 1350 keV deuteron beam for Li and C, respectively). The analyses required two or three different detectors. The charged particle annular detector, with a solid angle of 110 mSr mounted at a scattering angle of 170°, measured energies of backscattered and nuclear reactions induced particles: Rutherford Backscattering Spectrometry (RBS) and Nuclear Reaction Analysis (NRA) techniques. Two other detectors are available in the analysis chamber for X-rays and γ-rays detection. Typical X-rays and γ-rays spectra are shown in Fig. 5. The fluorine lithium and iron signals come from the matrix elements (active material $LiFePO_4$ and binder PVDF). Emission from a few other elements can also be seen in both spectra (Ca, Cr and Zn: from 50 to 1200 ppm). These impurities correspond generally to the ones present in the chemical precursors of iron used for the synthesis. Unfortunately, the $LiFePO_4$ with a carbon coating is a powder sold by two different companies; the synthesis method used is not disclosed, nor is the carbon coating process. Moreover, it appears that both active materials differ by the presence of a doping metal: vanadium or titanium (~2300 ± 55 ppm of V e.g. 0.23 at. % for LFP-A and ~2740 ± 238 ppm of Ti for LFP-B e.g. 0.28 at. %).

The method used to determine the content of lithium and the whole composition has been presented in details by Habrioux et al.[17] RBS technique is based on the fact that the energy of a backscattered particle depends on the mass of the target atom (kinematic factor) and on the depth at which the scattering took place (energy loss on the way to and from the point of interaction). Higher is the mass number Z, higher the detected energy of the backscattered particle is. The energy of the iron signal is then higher than the phosphorous signal,

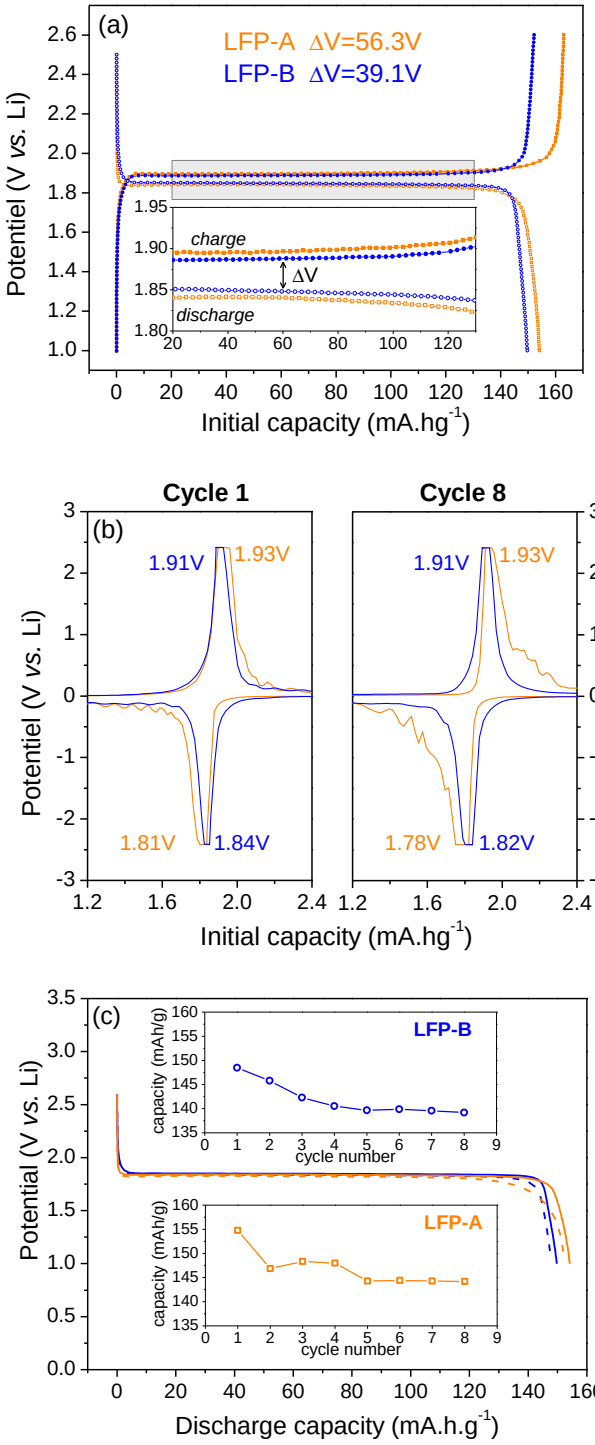


**Figure 3.** (a) Initial charge and discharge curves for two LFP electrodes. (b) Differential capacity dQ/dV vs potential for the firs and last cycles. (c) First (full line) and last (dashed line) potentiodynamic cycles at SOC 0%. The insets represent the discharge capacity as a function of cycles measured at C/10 regime for of full cell [$Li_4Ti_5O_{12}$/1 M $LiPF_6$ in EC-DMC/ LFP].

etc. As the ion beam techniques probes not only the surface of the sample but also the volume (for $LiFePO_4$ sample, the firs 50 μm are analyzed), the backscattered particle loses energy by passing through the material - before and after the collision with an atom A. The RBS spectra are thus composed of a succession of narrow peaks for a thin fil and steps for a thicker target (see suppl.info Fig. S1). The composition of the commercial powders is firs investigated, Rutherford

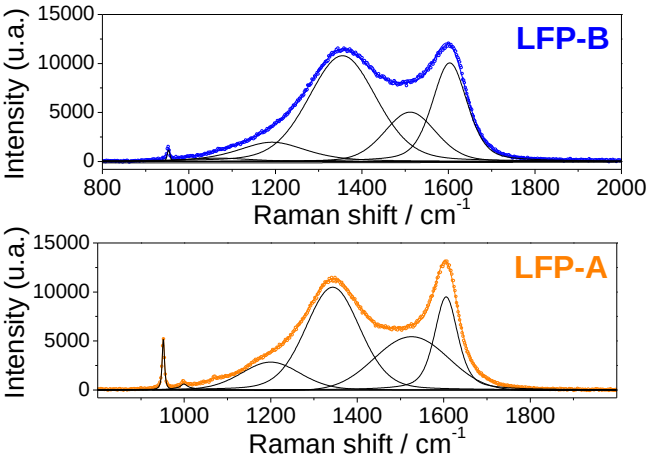


**Figure 4.** Comparison of experimental Raman spectra (symbol) and their deconvolution using a combination of four Gaussian - Lorentzian bands for two commercial C- $LiFePO_4$ materials.

Backscattering Spectra of powders and cathode materials for each company are represented in Fig. 6. The nominal composition of the powder C-$LiFePO_4$ is found. For the electrode analyses, the form of the signal corresponding to the carbon (near 1860 keV) is different for the two electrodes (Fig. 6b). For the LFP-A electrode, the signal is sharp: the composition of the electrode is not homogeneous along the section from the Al collector to the interface electrode/electrolyte. The spectrum is then simulated with two compositions: the firs composition is richer in carbon (near the interface, called layer 1) while the second contain less carbon (on the side of the Al collector, called layer 2), while an unique composition is used to simulate the LFP-B electrode. Using the SIMNRA program,[40] it is possible to estimate the thickness of the firs layer. The firs 23 nm of the interface electrode/electrolyte are richer in carbon (26.2 at. % instead of 11.1 at. %). Note that the energy of the ion beam analysis is unfortunately different between the analyses of the powders and the electrodes (2560 keV vs. 2600 keV). The form of the RBS spectra is therefore a little different (in the iron and phosphorous signals). The form depends of the cross section (i.e. the probability of interaction between the incident ion and the atom X in the target) of the backscattered particle and the energy of the incident ion. Moreover, the cross section must correspond to the geometry of the nuclear microprobe. In the simulation, the used cross section of the phosphorus atom is measured at 165°, while our geometry is 170°. We see some difference between the experimental and the simulated curves (especially beside the carbon signal for the spectra recorded at 2600 keV, but the phosphorus concentration stays correct.

In order to confir the carbon content in both electrodes, the deuteron microbeam at 1350 keV is used. The amount of carbon

**Table II. Refine parameters of the four bands used to fi the D (~1350 $cm^{-1}$) and G (~1600 $cm^{-1}$) bands of the experimental Raman spectra recorded for both commercial C-$LiFePO_4$ electrodes.**

| Materials | Raman peak ($cm^{-1}$) | FWHM ($cm^{-1}$) | $I_D/I_G$ | La(nm) | $sp^2/sp^3$ |
|---|---|---|---|---|---|
| LFP-A | 1199.8 | 158.2 | 2.55 | 1.9 | 1.39 |
| | 1343.1 | 146.3 | | | |
| | 1525.7 | 199.5 | | | |
| | 1605.8 | 61.9 | | | |
| LFP-B | 1191.9 | 179.1 | 2.07 | 2.4 | 2.76 |
| | 1354.6 | 182.1 | | | |
| | 1511.3 | 138.3 | | | |
| | 1603.4 | 93.2 | | | |

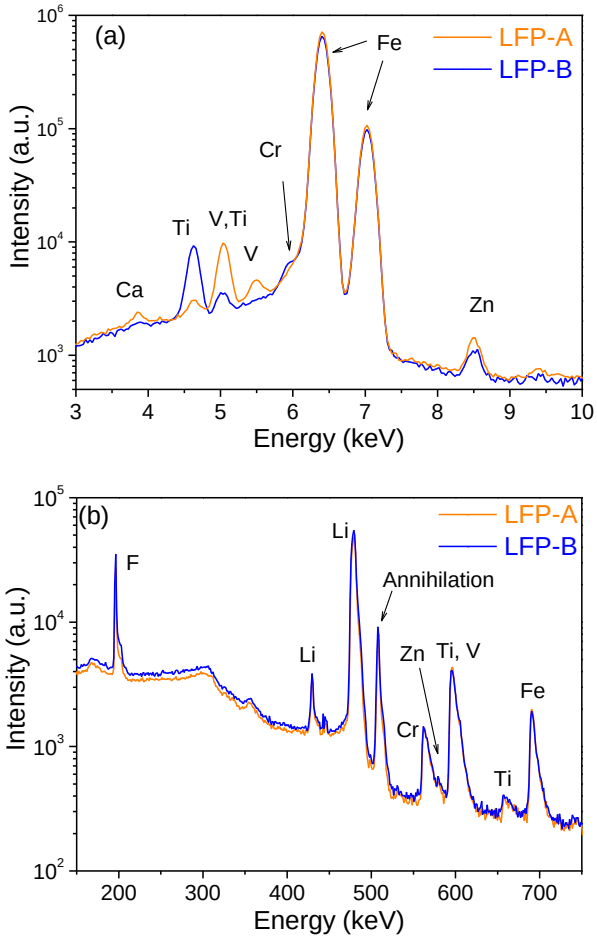


**Figure 5.** Typical X-ray (a) and γ-ray (b) spectra for $LiFePO_4$ materials obtained with a 2600 keV proton microbeam.

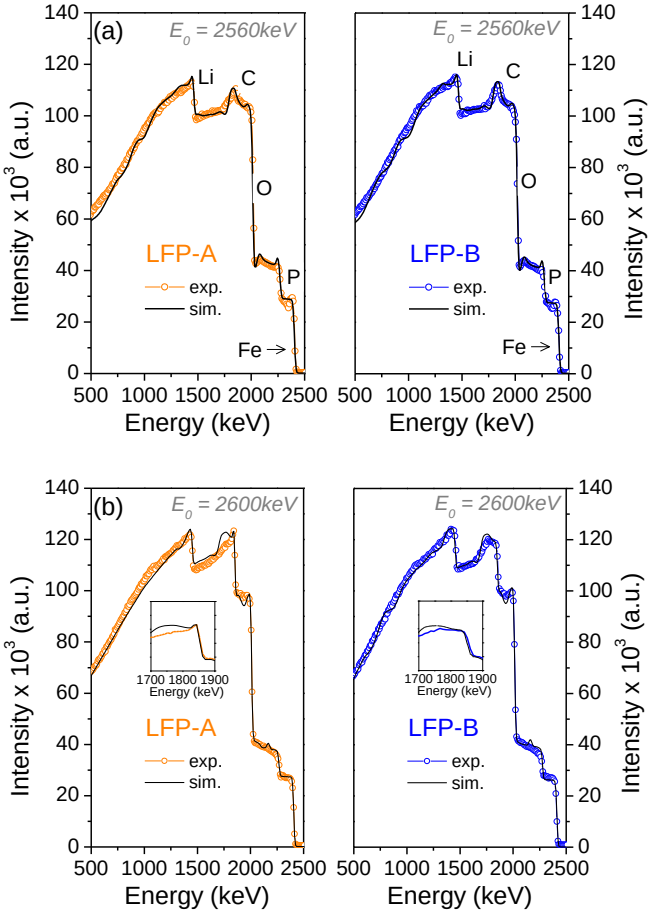


**Figure 6.** Rutherford Backscattering Spectra obtained with a $E_0$ keV protons beam of (a) $LiFePO_4$ coated commercial powders and (b) the associated pristine cathode materials.

composing the coating is estimated using the following relationship:

$$\frac{[C]}{[C_{ref}]} = \frac{S}{S_{ref}} \times \frac{A(C)}{A(C)_{ref}} \qquad [2]$$

where [C] and [$C_{ref}$] are respectively the concentrations of C element in the sample (stopping power S) and in a glassy carbon standard (stopping power $S_{ref}$). The stopping power corresponds to the distance that the incident ion runs through matter before stopping. A(C) and $A(C)_{ref}$ are respectively the normalized peaks areas associated with the nuclear reaction observed with C atom both in the sample and in the standard. Normalized spectra from LFP-A and LFP-B powders and electrodes are presented on Fig. 7a. If the analyzed target is thicker and homogeneous, the shape of the $^{12}C$ signal is proportional to the cross section of the $^{12}C(d,p_0)^{13}C$ nuclear reaction (inset). Here, we observe no difference for the powders, but we distinguish clearly the two contributions of the cross section for LFP-B and not for LFP-A electrodes: the presence of a layer richer in carbon is thus confirme for the LFP-A. Moreover, the peak of this reaction is larger for LFP-A electrode than for the LFP-B one: the repartition of the carbon is not uniform. LFP-A electrode has more carbon that LFP-B (including the carbon on the LFP coating, the carbon fibe and the binder). A comparison of calculated concentrations of carbon from deuterons and protons induced spectra is given in Fig. 7b. The evaluated carbon content is furthermore in agreement with the measurements made using the deuterons microbeam (20.8 at. % C and 18.1 at. % C for LFP-A and LFP-B respectively).

From the RBS and PIGE spectra analyses, we estimate the lithium content and the complete elemental concentrations. Fig. 8 shows the evolution of the lithium content during the charge process. The expected value of lithium is estimated based on the formulation of the electrode: 90.5 wt% active material, 5 wt% of VGCF fiber and carbon black, and 4.5 wt% of polyvinylidene fluorid (PVDF). As the content of the carbon coated is not disclosed for the commercial powders, we use the content estimated by ion beam technique. The concentrations of lithium in the commercial powders are in good agreement with the nominal composition of the active material $LiFePO_4$ with a carbon coating. The graph compares also the Li content estimated in a pristine electrode and a rinsed pristine electrode (electrode that is imbibed with electrolyte solution and rinsed with dimethylcarbonate to eliminate the residual electrolyte). The results confir that cleaning process employed to remove electrolyte solution is well adapted (the same values are obtained before the cycling). We observe less lithium content that expected for LFP-A. A deviation of the formulation of the electrode may cause a lower concentration, but it is within the errors bars. During the charge/discharge of the battery, the content of lithium is closer to the lithium content predicted by electrochemistry (Fig. 8). As soon as the battery is working, an immobilization of the lithium occurs for the LFP-B electrodes. This tendency is not clear for the LFP-A electrodes. The evolution of the lithium content seems to follow the electrochemical prevision except for the last two points.

Using the dedicated program RISMIN,[40] it is possible to draw the lithium distribution, from the reaction $^7Li(p,p'\gamma)^7Li$ of PIGE spectra at 478 keV. Fig. 9 compares the RBS and PIGE spectra for the SOC 75% of LFP-A and LFP-B electrodes in the full map and in a specifi region of interest. We can see clearly some heterogeneous areas, which explain partially the difference of lithium concentration determined by ion beam techniques. The lithium clusters (surrounded) are 45% and 22% richer in lithium than in the total region for respectively

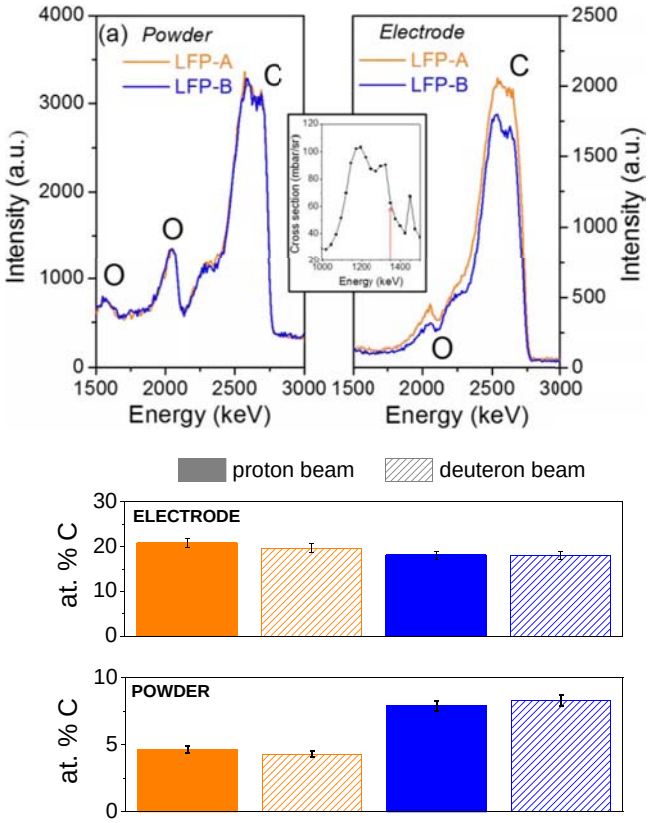


**Figure 7.** (a) Spectra obtained with a deuteron microbeam at the energy of 1.35 MeV with both LFP-A (orange line) and LFP-B (blue line) in powder and electrode materials. A 25 μm Mylar foil is set in front of the annular detector. The inset represents the cross section of the $^{12}C(d,p0)^{13}C$ nuclear reaction. Carbon maps drawn using the $^{12}C(d,p0)^{13}C$ nuclear reaction are also represented. (b) Carbon concentrations (in at. %) obtained with deuteron (no pattern) and proton beams (with dense pattern).

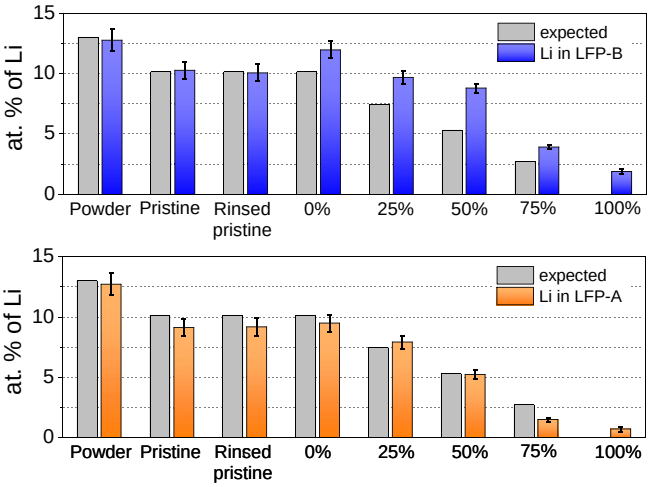


**Figure 8.** Comparison of experimentally determined and expected concentrations of lithium (in at. %) in C-$LiFePO_4$ active powder and electrode materials for both companies.

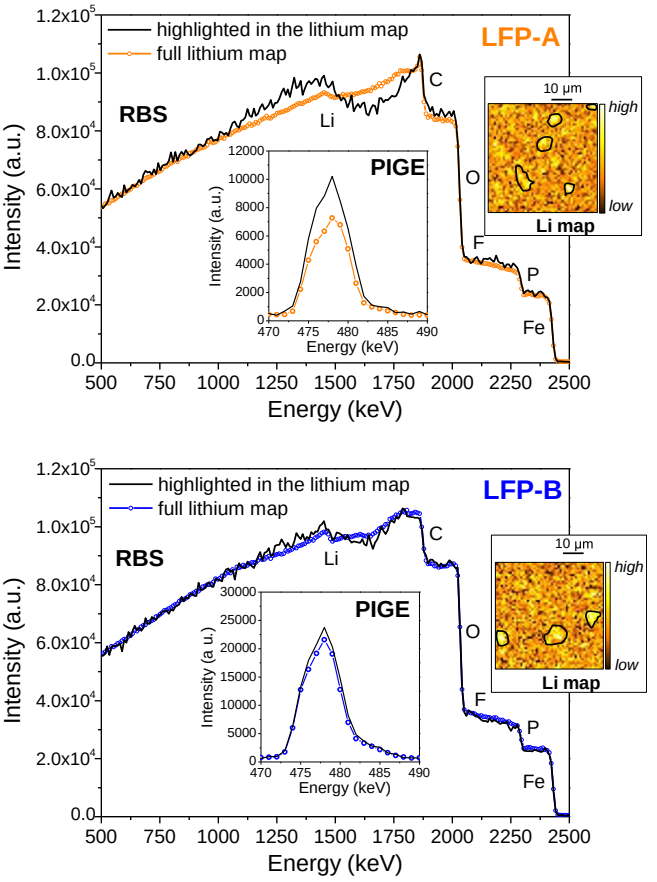


**Figure 9.** Full RBS (symbol) and local RBS (line) spectra obtained with intensities coming from selected ROI in LFP-A and LFP-B at SOC 75%. Lithium cluster are highlighted in the lithium maps, represented in insets.

LFP-A and LFP-B. Unfortunately, due to the small region of interest considered (<5% of the full region), the statistics are very poor and it is thus not possible to estimate with a good accuracy the full composition of the clusters. It is worth noting that these clusters cannot explain the deviation of lithium content.

## Summary

The investigation of the structural and physical properties of two commercial $LiFePO_4$ powders with different carbon coatings have provided us a better understanding of the role of the carbon coating. The Rietveld refinement show that iron environment is completely ordered in the two structures. The analyses of the carbon D and G bands in the Raman spectra gives information about the carbon coating. LFP-B is more graphitized than LFP-A, which appears amorphous. The real composition of the active materials was not disclosed by the two companies. However, Ion beam techniques allow us to estimate the carbon content and the metal doping in the powder materials. Two doping metal are identified vanadium and titanium for LFP-A and LFP-B respectively). The nature and the content of the carbon coating in the powder are also different (4.5 at. % and 8.1 at. % for LFP-A and LFP-B respectively). RBS spectra recorded for the LFP-A electrode show that the carbon composition along the cross section (from the collector to the electrode/electrolyte interface) is not homegeneous: a layer richer in carbon is observed at the electrode/electrolyte interface. On the other hand, the composition of the LFP-B electrode is homogeneous. The lithium and carbon content distributions have also been investigated using IBA techniques. In both cases, an immobilization of lithium is observed. This immobilization is more significan for the LFP-B material. We cannot conclude exactly on the role of the metal doping or on the nature of the carbon coating in the formation of the richer layer observed on LFP-A electrodes. However, the nuclear microanalysis appears as a powerful tool to visualize the lithium cluster in the electrodes cycled at different states of charge.

## Acknowledgment

The authors thank the nanoscience program of CEA for funding within the frame of ChimTronique subprogram. We are also grateful to Didier Guillier and Yvan Kilisky for the accelerator operation.


## References


1 A K Padhi, K S Nanjundaswamy, and J B Goodenough, *J. Electrochem. Soc* , **144**, 1188 (1997)
2 C Wang, U S Kasavajjula, and P E Arce, *J. Phys. Chem. C*, **111**, 16656 (2007)
3 A Yamada, S C Chung, and K Hinokuma, *J. Electrochem. Soc.*, **148**, A224 (2001)
4 A Marongiu and D U Sauer, *Int. J. Automot. Technol.*, **17**, 465 (2016)
5 P S Herle, B Ellis, N Coombs, and L F Nazar, *Nat. Mater* , **3**, 147 (2004)
6 J Lu, G Oyama, S Nishimura, and A Yamada, *Chem. Mater.*, **28**, 1101 (2016)
7 K -M Kang, H -W Kim, and H -Y Kwak, *Korean J. Chem. Eng.*, **33**, 688 (2016)
8 C Delacourt, P Poizot, S Levasseur, and C Masquelier, *Electrochem. Solid-State Lett* , **9**, A352 (2006)
9 X Huang et al , *Mater. Charact.*, **61**, 720 (2010)
10 R Malik, D Burch, M Bazant, and G Ceder, *Nano Lett* , **10**, 4123 (2010)
11 G Zeng, R Caputo, D Carriazo, L Luo, and M Niederberger, *Chem. Mater* , **25**, 3399 (2013)
12 W -J Zhang, *J. Power Sources*, **196**, 2962 (2011)
13 D H Nagaraju, M Kuezma, and G S Suresh, *J. Mater. Sci.*, **50**, 4244 (2015)
14 F Kang, J MA, and B LI, *New Carbon Mater.*, **26**, 161 (2011)
15 B L Cushing and J B Goodenough, *Solid State Sci.*, **4**, 1487 (2002)
16 N Dupré et al , *J. Power Sources*, **195**, 7415 (2010)
17 A Habrioux et al , *Nucl. Instrum. Methods Phys. Res. Sect. B Beam Interact. Mater. At.*, **290**, 13 (2012)
18 R Gonzalez-Arrabal et al , *J. Power Sources*, **299**, 587 (2015)
19 J Rodriguez-Carvajal, *Abstr. Satell. Meet. Powder Diffr. XV Congr. IUCr*, 127 (1990)
20 D -H Kim and J Kim, *Electrochem. Solid-State Lett.*, **9**, A439 (2006)
21 J Chen and M S Whittingham, *Electrochem. Commun.*, **8**, 855 (2006)
22 Y -D Cho, G T -K Fey, and H -M Kao, *J. Power Sources*, **189**, 256 (2009)
23 C -W Ong, Y -K Lin, and J -S Chen, *J. Electrochem. Soc.*, **154**, A527 (2007)
24 R Kostecki et al , *Thin Solid Films*, **396**, 36 (2001)
25 R E Shroder, R J Nemanich, and J T Glass, *Phys. Rev. B*, **41**, 3738 (1990)
26 C M Burba and R Frech, *J. Electrochem. Soc.*, **151**, A1032 (2004)
27 T Nakamura, Y Miwa, M Tabuchi, and Y Yamada, *J. Electrochem. Soc.*, **153**, A1108 (2006)
28 C M Julien et al , *J. Appl. Phys* , **100**, 063511 (2006)
29 P Lespade, A Marchand, M Couzi, and F Cruege, *Carbon*, **22**, 375 (1984)
30 R Al-Jishi and G Dresselhaus, *Phys. Rev. B*, **26**, 4514 (1982)
31 R E Shroder, R J Nemanich, and J T Glass, *Phys. Rev. B*, **41**, 3738 (1990)
32 M Veres, S Tóth, and M Koós, *Diam. Relat. Mater.*, **17**, 1692 (2008)
33 M M Doeff, J D Wilcox, R Kostecki, and G Lau, *J. Power Sources*, **163**, 180 (2006)
34 L C Nistor et al , *Appl. Phys. A*, **58**, 137 (1994)
35 L E McNeil, J Steinbeck, L Salamanca-Riba, and G Dresselhaus, *Carbon*, **24**, 73 (1986)
36 F Tuinstra and J L Koenig, *J. Chem. Phys.*, **53**, 1126 (1970)
37 C Benybassez and J Rouzaud, *Scan. Electron Microsc* , 119 (1985)
38 M Maccario et al , *J. Electrochem. Soc.*, **155**, A879 (2008)
39 K A Seid et al , *J. Mater. Chem.*, **22**, 2641 (2012)
40 M Mayer, J L Duggan, B Stippec, and I L Morgan, in *AIP Conference Proceedings*, **475**, 541, AIP (1999)